DOI: 10.1002/ejic.200701122

Studies on Nickel(II) Complexes with Amide-Based Ligands: Syntheses, Structures, Electrochemistry and Oxidation Chemistry

Jyoti Singh,[a] Geeta Hundal,[b] and Rajeev Gupta*[a]

Keywords: Nickel / N ligands / Structure elucidation / Electrochemistry / Oxidation

The present work discusses the nickel chemistry in a set of amide-based open-chain ligands with subtle differences in the backbone or terminal amine substituents. The ligands coordinate to the Ni^{2+} ion through the N_{amide} and N_{amine} atoms maintaining a square-planar geometry. Absorption spectra and NMR studies reveal that the solid-state square-planar geometry is retained in solution. The electrochemical results suggest that the Ni^{III}/Ni^{II} redox couple primarily depends on the N_4 donors, which is composed of two N_{amide} and two N_{amine} atoms and not on the peripheral substituents. All four ligands with variable backbone and substituents are equally competent in stabilizing the Ni^{III} state. On the basis of electrochemical findings, chemical oxidations were carried out, and they reveal generation of the Ni^{III} state in two cases, whereas decomposition was observed in others. Preliminary alkene epoxidation reactions suggest that the present nickel complexes transiently stabilize the higher oxidation state of the nickel ion that possibly participates in the oxidation of the substrates.

Introduction

The interests in the coordination chemistry of nickel in variable oxidation state(s) with synthetically designed ligands is an area of considerable significance with implications in chemistry and biology.[1] Our understanding about nickel biological systems has tremendously been enlightened after the recent spectroscopic and structural investigations of the active-site structure from certain microorganisms.[2] As a result of their biological significance as biomimetic models, as well as their potential application in catalytic oxidation reactions,[3] the field of high-valent nickel chemistry has continued to grow. In addition, the involvement of Ni^{III} species in a number of enzymes, such as [Ni–Fe] hydrogenases,[4] Ni superoxide dismutase,[5] Ni^{I}/Ni^{III} species in CO dehydrogenases[6] and acetyl coenzyme-A synthase,[7] demands special attention on the redox chemistry of the nickel ion. In this context, designed organic ligands hold potential with the unique ability to modulate the redox chemistry of the nickel ion.[8] The ligand architecture and its mode of coordination[9] is an important factor responsible for the redox regulation of a metal centre, and the present work is an attempt to understand the effect of the macrocyclic versus open-chain nature of the ligands on the structure and redox chemistry of the nickel ion.

The effect of the macrocyclic versus open-chain nature of the ligands on the metal ions, in particular nickel, was always considered to be an important feature and has been frequently addressed.[10] A considerable amount of work has also been done on the saturated tetraaza systems both with macrocyclic as well as open-chain ligands.[11] Lampeka and coworkers[12,13] through their elegant comparative studies on the dioxotetraaza systems have demonstrated the significant changes in the structural, absorption spectral and the redox properties of the nickel complexes caused by the macrocyclic versus open-chain nature of the ligands.

Recently, we[14] showed nickel chemistry in a set of amide-based macrocyclic ligands while keeping the primary coordination sphere as well as the cavity size of the macrocycle fixed (Scheme 1). These macrocyclic ligands have been shown to stabilize the +2 as well as +3 (transiently) oxidation states of the nickel ion in a square-planar geometry. The present work stems from our search to prepare and study nickel complexes in an analogous non-macrocyclic ligand environment, and we have commenced a systematic investigation to shed some light on the differences imposed by the macrocyclic ligands versus open-chain ligands. Herein, we report the design and synthesis of four open-chain amide-based ligands and their coordination chemistry towards the Ni^{II} ion (Scheme 2). The ligands were designed in a way to keep the primary donor environment around the metal centre identical, so that the effect of the open-chain versus macrocyclic nature of the ligands on the physical, structural, spectroscopic and redox properties of the nickel centre could be evaluated. Furthermore, we also show the Ni^{II}-catalyzed epoxidation of the alkenes, which

[a] Department of Chemistry, University of Delhi, Delhi, 110007 India
Fax: +91-11-2766-6605
E-mail: rgupta@chemistry.du.ac.in
[b] Department of Chemistry, Guru Nanak Dev University, Amritsar, 143005 Punjab, India

Supporting information for this article is available on the WWW under http://www.eurjic.org or from the author.

thus attests to the ability of the present nickel complexes to transiently stabilize higher oxidation states to promote oxidation.

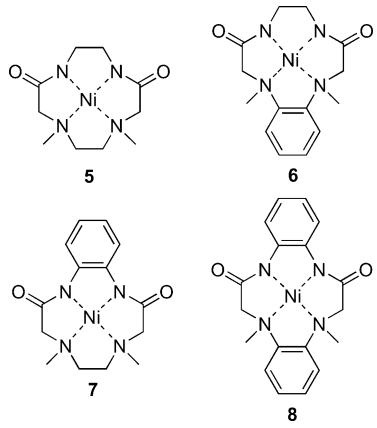

Scheme 1. Ni^{II} complexes of macrocyclic ligands.

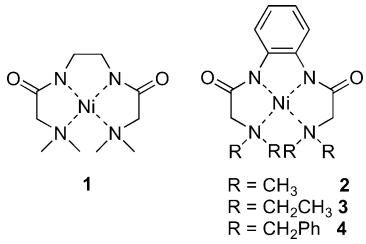

Scheme 2. Ni^{II} complexes of open-chain ligands.

Results and Discussion

Ligand Design and Synthesis

All four open-chain ligands, H_2L^1–H_2L^4, are designed to simultaneously provide coordination through two amide and two amine atoms while maintaining an identical primary coordination environment around the nickel centre. The only difference is the substituents used at the N_{amine} end with the possibility to alter the electronic and steric factors. The ligand H_2L^1 however, differs from the rest due to the involvement of a flexible ethylene backbone whereas other three ligands incorporate rigid *o*-phenylene backbone as part of the ligand. These ligands were synthesized in two steps starting from the desired primary diamines. The primary diamine was first converted into the bis(chloroacetamide),[14] which was further treated with the secondary amine (dimethyl-, diethyl- or dibenzylamine) to afford the final ligands. During the synthesis of these ligands, an excess amount of the secondary amine was used, which also functioned as a base in the reaction. All new ligands were thoroughly characterized by using various spectroscopic measurements and gave satisfactory microanalyses results.

Synthesis and Characterization of Nickel Complexes

All four Ni^{II} complexes, **1**–**4**, were synthesized by treating the DMF solution of the ligand with solid NaH under an N_2 atmosphere followed by the addition of $NiCl_2$ [or $(Et_4N)_2NiCl_4$ for **4**]. Usual workup and recrystallization [vapour diffusion of diethyl ether into either a CH_2Cl_2 (for **1** and **3**), DMF (for **2**) or MeCN (for **4**) solution] afforded a highly crystalline material in good recrystallized yield (60–80%). Whereas complexes **1**–**3** are deep-yellow to orange in colour, complex **4** is brown.

In the FTIR spectra, the absence of the ν(N–H) stretching frequency and the observed bathochromic shift in the $C{=}O_{amide}$ stretch relative to the free ligand confirms the involvement of the deprotonated amidate group in the bonding.[14,15] Complexes **1** and **4** also have water as the solvent of crystallization, which shows the ν(OH) absorption in the region of 3210–3430 cm^{-1}.[15] Solution conductivity[16] data confirm the nonelectrolytic nature of all four complexes, whereas the elemental analysis results authenticate the purity of the bulk samples. In the electrospray mass spectra, the molecular ion peak corresponding to complexes **1**, **2**, **3** and **4** was obtained at 287.08 $[M + H]^+$, 357.69 $[M + Na]^+$, 392.80 $[M + H]^+$ and 639.76 $[M + H]^+$, respectively, which thus confirms the integrity of the nickel complexes in the solution.

Crystal Structure Studies

Representative complexes **2** and **4** were also characterized by X-ray structure analysis, and their molecular structures are shown in Figures 1 and 2 (see Figure S1 for complete numbering scheme of **4**), whereas the important crystallographic and structural details are contained in Tables 1, 2 and 5. The nickel ion is coordinated by two anionic N_{amide} atoms and two neutral N_{amine} centres in a square-planar geometry as also noted for macrocyclic analogues **5**–**8**.[14] In both complexes, the Ni^{II} centre is surrounded by three five-membered chelate rings.

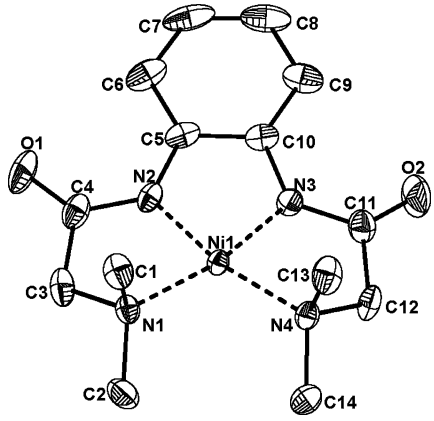

Figure 1. Molecular structure of complex **2**. Thermal ellipsoids are drawn at 30% probability level. Hydrogen atoms are omitted for clarity.

For complex **2**, the average $Ni–N_{amide}$ distance of 1.842(2) Å is 0.144 Å shorter than the average $Ni–N_{amine}$ distance of 1.986(2) Å. This difference may be attributed to the anionic coordination from the deprotonated N_{amide}

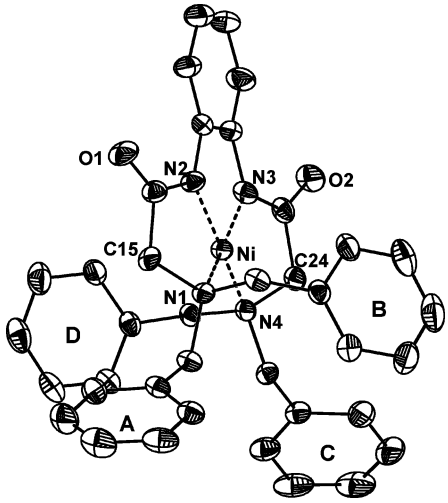

Figure 2. Molecular structure of complex **4** with partial numbering scheme. Thermal ellipsoids are drawn at 30% probability level. Solvent molecule and hydrogen atoms are omitted for clarity.

Table 1. Selected bond lengths [Å] and angles [°] for [Ni(L^2)] (**2**) and [Ni(L^4)] (**4**).

Distance/Angle	[Ni(L^2)] (**2**)	[Ni(L^4)] (**4**)
Ni–N1	1.982(2)	2.034(4)
Ni–N2	1.844(2)	1.859(4)
Ni–N3	1.840(2)	1.851(4)
Ni–N4	1.990(2)	2.022(4)
N2–Ni–N3	84.24(10)	84.32(18)
N3–Ni–N4	84.24(9)	83.28(17)
N2–Ni–N4	167.96(10)	164.69(18)
N1–Ni–N3	168.52(9)	163.68(16)
N1–Ni–N2	85.10(10)	82.77(17)
N1–Ni–N4	106.09(9)	110.90(16)

donors instead of the neutral donation from the N_{amine} groups. A similar observation was noticed for the macrocyclic analogue (complex **7**)[14] of this complex (Table 2). The bond angles formed by the five-membered chelate rings are smaller than 85° and indicate a tight chelation to the nickel ion. The N_{amine}–Ni–N_{amine} bite angle at 106.09(9)° is quite spread out and at least 20° larger than the other N–Ni–N angles. The nickel ion is 0.072 Å displaced from the N_4 basal plane (defined by N1, N2, N3 and N4). Two lateral five-membered chelate planes make an angle of ca. 15° with each other, whereas they make an angle of 6–11° with the central five-membered chelate ring involving two N_{amide} groups. The C3 and C12 carbon atoms are significantly out of their respective chelate planes as seen by the N1–C3–C4–N2 and N4–C12–C11–N3 dihedral angles, respectively. The small dihedral angle of ca. 1.6° for the N2–C5–C10–N3 fragment indicates the planarity induced by the rigid *o-phenylene* part. This structure is in complete agreement with that of **7** and in contrast to that of **5** and **6** where a flexible *ethylene* fragment was the part of the macrocyclic ligand.[14]

For **4**, the average Ni–N_{amide} and Ni–N_{amine} distances at 1.855(4) Å and 2.028(2) Å are 0.013 Å and 0.042 Å longer than the similar distances in complex **2** (Table 2). The difference between the amide and amine donors is 0.173 Å. The bond angles formed by the five-membered chelate rings are within 83–84° and are at least 27° smaller than the N1–Ni–N4 angle. In particular, the N_{amine} centres have stretched out appreciably possibly due to bigger benzyl substituents attached to it. The nickel ion is almost within the N_4 basal plane with a displacement of only 0.009 Å. All five-membered chelate planes make angles of 9–13° with each other as also seen for **2**. The C15 and C24 carbon atoms are significantly out of their respective chelate planes as also noticed in **2**. The four N atoms are almost planar with average deviation of 0.1 Å from the plane; however, quite significant deviations for the two N_{benzyl} centres lead them to be displaced opposite to each other. This displacement has resulted in the unique arrangement of the attached phenyl rings. Two phenyl rings **A** (C2 to C7) and **B** (C9 to C14) on N1 and **C** (C26 to C31) and **D** (C33 to C38) on N4 are nearly *gauche* to each other (dihedral angles of 47 and 58°, respectively). Although **A** and **C** are *gauche* (dihedral angle 69°), **B** and **D** are *syn* to each other (dihedral angle 16°). Thus, **A** and **C** face outwards away from each other and the metal ion, but **B** and **D** become parallel to each other and face the metal ion. The latter give rise to cation···π interactions with the metal ion, and the phenyl rings **B** and **D** have average centroid-to-metal-ion distance of ca. 3.8 Å.[17] Thus, these two phenyl rings may be considered to form two long bonds that occupy the fifth and sixth coordination positions in a distorted octahedron around the metal ion (Figure S2). Furthermore, the distance between the Ni ion and the benzylic carbon centres ranges from 2.824 to 3.076 Å and the possibility of weak agostic and/or M···H–bond interactions cannot be ruled out. Similar interactions were observed for the coordination complexes in the literature.[18]

Weak C–H···X H-bonding interactions (Table S1) create an interesting crystal structure. Phenylene C35 and methylene C32 H-bonds with amide oxygen O2 of the centrosym-

Table 2. Comparative structural parameters of open-chain (**2** and **4**) and macrocyclic Ni^{2+} complexes **5**–**8**.

Complex	Average Ni–N_{amide} [Å]	Average Ni–N_{amine} [Å]	N_{amide}–Ni–N_{amide} [°]	N_{amine}–Ni–N_{amine} [°]	Displacement of Ni out of N_4 basal plane [Å]
2[a]	1.842(2)	1.986(2)	84.24(10)	106.09(9)	0.072
4[a]	1.855(4)	2.028(4)	84.32(18)	110.90(16)	0.009
5[b]	1.807(3)	1.906(3)	87.40(11)	92.36(11)	0.170
6[b]	1.818(4)	1.910(4)	87.90(12)	92.08(12)	0.136
7[b]	1.803(2)	1.890(2)	87.24(10)	92.44(11)	0.126
8[b]	1.814(4)	1.898(4)	87.47(18)	91.95(17)	0.110

[a] This work. [b] Ref.[14]

metrically related molecules forming a 1D linear polymeric chain running parallel to the *b* axis in the *ab* plane (Figure 3). Within this chain two centrosymmetric **D** phenyl rings come close to each other and display π···π interactions between them with a centroid-to-centroid distance of ca. 3.8 Å. This π···π interaction further stabilizes the formation of an H-bonded 1D polymer.

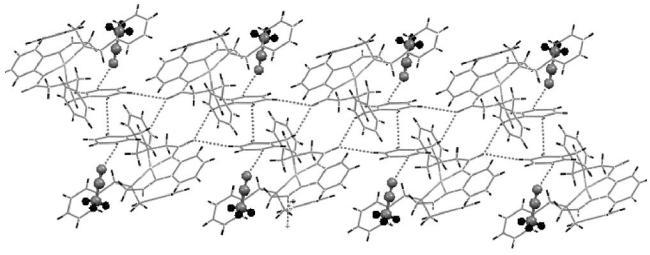

Figure 3. Molecular structure of complex **4** showing the H-bonding interactions, π···π interactions and solvent molecule (CH_3CN, shown in ball-and-stick fashion), in the *ab* plane along the *b* axis. See text for details.

Amide oxygen O2 is also H-bonded to phenylene C28 of a symmetry-related molecule along the *a* axis in the *ab* plane, which thus links two such parallel chains along the plane. Hence, the O2 atom behaves as a triple H-bond acceptor and is responsible for the 2D extension of the polymer. The acetonitrile solvent molecule is held between two such chains by various H-bonding interactions. Each solvent molecule acts as a double H-bond donor through its methyl group and quadruple H-bond acceptor through the C3, C13, C20 and C37 phenylene carbon atoms. Thus, any two parallel polymeric chains are linked to each other through the solvent molecule and also through C4···O1 H-bonding interactions. Out of these, the C51···O1 and C37···N50 interactions propagate the crystal structure along the *c* axis to extend it in a third dimension along the *bc* plane (Figure S3).

The observed Ni–N_{amide} distances for the present Ni^{II} complexes are within the range of other structurally characterized cases including the Ni^{2+} complexes of Vagg and coworkers,[19] Fenton and coworkers[20] and Journaux and coworkers (with tetraamide ligands).[21] However, these distances are ca. 0.02–0.05 Å longer than those in the Ni^{II} complexes of the macrocyclic ligands, **5**–**8**.[14] Furthermore, these distances are marginally longer than the 13-membered and ca. 0.03 Å smaller than the 14-membered macrocyclic dioxotetraaza nickel complexes of Lampeka and coworkers.[12a,12b]

Absorption Spectral Studies

The absorption spectra of complexes **1**–**4** were studied in a number of solvents, such as, MeCN, DMF, DMSO and H_2O. A comparative spectrum in MeCN is shown in Figure 4, whereas other spectra are part of the Supporting Information (Figures S4a and S4b). The λ_{max} as well as other prominent features were found to remain invariant to changes in solvent polarity or the coordinating ability. The complexes were also titrated with other potential axial ligands, such as Cl^-, ClO_4^-, pyridine and 4-dimethylaminopyridine, and no change in the spectral features was observed. These experiments strongly suggest that the nickel centre remains four-coordinated. Noteworthy is that the analogous copper(II) complex of ligand H_2L^2 [$Cu(L^2)$] shows the axial coordination either from the O_{amide} atom of the neighbouring molecule in the solid state or from the solvent in solution.[22]

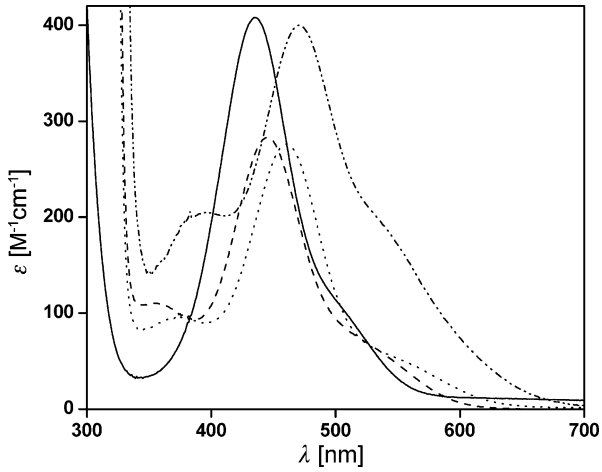

Figure 4. UV/Vis spectra of nickel complexes in CH_3CN: complex **1** (——), **2** (-----), **3** (·····) and **4** (-···-·-).

The λ_{max} was observed from 435 to 470 nm, and it was accompanied by a low-energy shoulder in the range 515–570 nm. The low ε value for these features suggests the d–d transition nature of the peaks. The high-energy features are apparent below 310 nm and could tentatively be assigned to intraligand charge-transfer bands. The observed similarity between the spectral features of the nickel complexes is also reflected in their very similar solid-state crystal structures (for **2** and **4**) as well as their proton and carbon NMR spectra (vida infra). The λ_{max} for complexes **1** and **2** are quite close to their macrocyclic analogues (complexes **5** and **7**, respectively),[14] whereas the absorption maxima differ for **3** and **4** and suggest that the incorporation of the sterically demanding groups (ethyl or benzyl) tend to alter the chromophore. In fact, the λ_{max} shifts to lower energy for **3** and **4** than for **1** and **2** (and **5** and **7** as well) and point out a weaker ligand field strength around the nickel centre.

NMR Spectral Studies

To investigate the solution state structures of the nickel complexes, ^1H and ^{13}C NMR spectroscopic studies were performed (Figure S5 and S6). All four complexes, **1**–**4**, are diamagnetic with $S = 0$ ground state as displayed by their sharp and ligand-like NMR spectra. Assignments of the signals were made through consideration of the relative peak area and comparison with the spectrum of the free ligand. The interesting aspect of the proton spectra of **3** and **4** is the observation of the AB-type or *geminal* coupling[12] for the $–CH_2R$ group (where R = CH_3 for **3**, and Ph for **4**)

due to the diastereotopicity of the methylene protons. Two methylene protons were observed at two different positions for these two complexes. In the case of **3**, the pair of protons were observed as multiplets at ca. 2.92 and ca. 2.45 ppm. The multiplicity is most likely caused by the presence of the methyl group as the immediate neighbour. The adjacent methyl groups appear as triplets (J = 7.0 Hz). For **4**, the pair of protons appear as doublets at δ = 2.59 and 3.66 ppm with $J(H^AH^B)$ of ca. 12 Hz.

The ^{1}H NMR spectra for nickel complexes **1**–**4** are much simpler than those of their macrocyclic analogues (**5**–**8**).[14] This is most likely due to the absence of the structural rigidness, as the chelate rings invert much more rapidly, which results in a simple time-averaged spectrum. For example, no AB-type coupling was observed for the protons attached to the –C(O)CH$_2$– group, which was a unique feature for all four macrocyclic Ni^{II} complexes, **5**–**8**.[14] In addition, the ^{13}C NMR spectra of **1**–**4** are quite straight forward and a close similarity in the chemical shifts of the identical carbon centres was clearly noticeable (Figure S6). Importantly, the NMR spectroscopic studies reveal that the solid-state conformation of the nickel complexes is retained in the solution state.

Electrochemical Studies

In order to obtain information about the accessibility of the Ni^{III} state and/or possible ligand oxidation, cyclic voltammetric (CV) and controlled-potential electrolysis (coulometry) experiments were performed on all Ni^{II} complexes. The electrochemical experiments were done in CH$_3$CN as well as in the better-coordinating and more-polar solvent DMF. All potentials (in V) are reported versus saturated calomel electrode (SCE) throughout the text (Table 3).

Table 3. Electrochemical data for [Ni(L^1)] (**1**), [Ni(L^2)] (**2**), [Ni(L^3)] (**3**) and [Ni(L^4)] (**4**) and their comparison with macrocyclic complexes **5**–**8**.

Complex	E_1[a]	E_2[a]	E_3[a]	E_1[b]	E_R[a]	Ref.
1	0.75	–	–	0.65	–	this work
2	0.82[c], 0.90	1.10	–	0.82[c]	–1.86	this work
3	0.80[c]	1.00[c]	–	0.80[c]	–1.80	this work
4	0.78[c]	1.14[c]	1.71[c]	0.78[c]	–1.67	this work
5	0.61	–	–	0.53	–	[14]
6	0.78	1.88	–	0.67	–	[14]
7	0.71	1.10	–	0.67	–	[14]
8	0.83	1.13	1.32[c]	0.78	–	[14]

[a] Solvent: CH$_3$CN; Complex ca. 1 mM solution, TBAP as supporting electrolyte ca. 100 mM solution, potential vs. SCE, glassy-carbon working electrode, Pt auxiliary electrode, scan rate = 100 mV s^{-1}. [b] Solvent: DMF, other parameters as in [a]. [c] E_{pa}.

Electrochemistry in CH$_3$CN

Quasireversible to irreversible responses were observed when the CV studies were performed in CH$_3$CN on the glassy carbon or platinum working electrode. Complex **1** showed only one oxidative response at 0.75 V with peak-to-peak separation (ΔE_p) of 100 mV (Figure 5). The coulometry experiment confirmed the 1e$^-$ nature of this response. Complex **2** displays three redox processes at 0.82 (E_{pa}), 0.90 (ΔE_p = 50 mV) and 1.1 V (ΔE_p = 60 mV) (Figure 6). The number of coulombic electron count was found to be collectively one for the first two responses. We believe that the first two redox processes are metal-based, whereas the third one is located on the ligand (vide infra). The first redox response, however, disappeared after the coulometric oxidation at 1.0 V, and the remaining two processes now appear as chemically reversible processes observable at 0.90 and 1.1 V (Figure 6). The coulometric oxidation at 1.35 V also resulted in the identical observation that the two responses are now reductive in nature. The exact nature of the species responsible for the feature at 0.82 V is not clear to us.[23] Complex **3** shows completely irreversible features (E_{pa}) at 0.8 and ca. 1.0 V with 1e$^-$ nature of each process (Figure S7). There is, however, another response at ca. 1.6 V that we believe is due to some electrochemically generated species. Three irreversible redox processes (all E_{pa}) were ob-

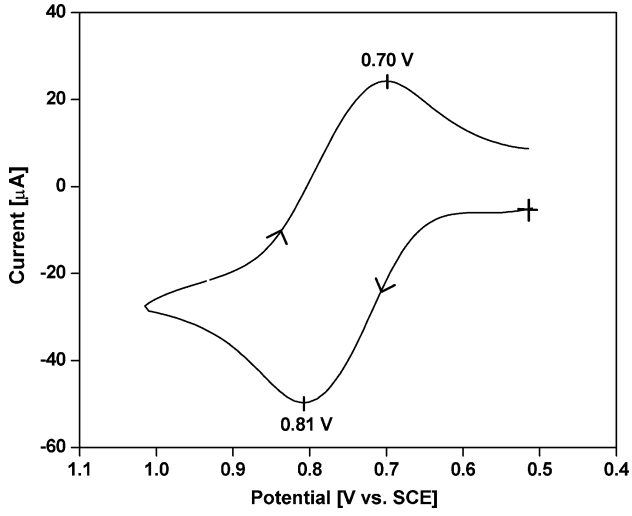

Figure 5. Cyclic voltammogram of complex **1** in CH$_3$CN.

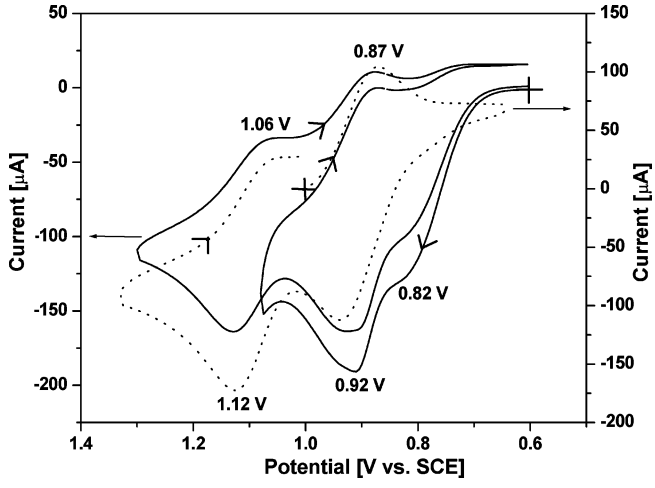

Figure 6. Cyclic voltammograms of complex **2** in CH$_3$CN before (——) and after (·····) coulometric oxidation at 1.0 V.

served at 0.78, 1.14 and 1.71 V for complex **4** (Figure 7). The one-electron nature of each redox process was again confirmed by the coulometric studies.

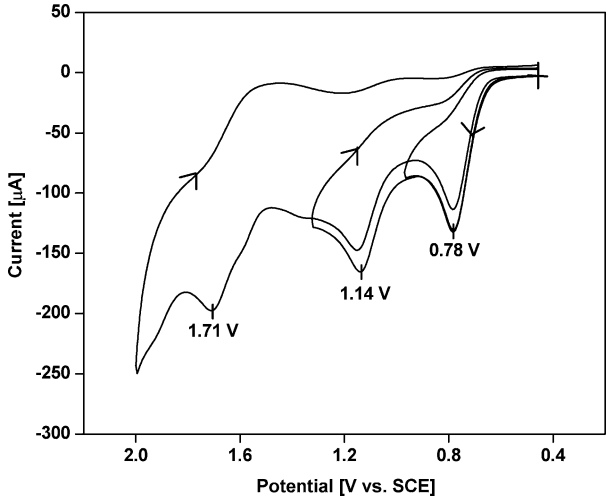

Figure 7. Cyclic voltammogram of complex **4** in CH_3CN.

The E_1 potentials (the first redox process) for all four Ni^{II} complexes come in a small potential window of 0.75–0.90 V. This process is most likely based on the nickel centre. The reason for a narrow potential window is due to the identical primary donor groups composed of two anionic N_{amide} and two neutral N_{amine} atoms. The E_1 potential for macrocyclic analogues **5**–**8** were in the range 0.61–0.83 V under identical experimental conditions.[14] The observed similarity in the E_1 potential suggest that the Ni^{II} state is evenly stabilized by the open-chain relative to the macrocyclic systems. Similarly, the E_2 potentials (the second redox process) also fell within the small range 1.0–1.15 V for complexes **2**–**4**. The E_2 potentials for macrocyclic analogues **6**–**8** were between 1.10–1.13 V that we had assigned as the oxidation of the *o-benzenediamidate* fragment generating the Ni^{3+}-*o-benzosemiquinonediimine π-cation* species.[14,21,24] On the basis of the similarity of the two classes of compounds, we suggest that the E_2 process is based on the ligand. Complex **4**, however, shows a third process, E_3 at 1.71 V that we tentatively assign as the oxidation of the benzyl substituents.

The +3/+2 reduction potentials (E_1) for the Ni^{II} square-planar complexes determined in this work are on the higher side relative to that of the tetraamidate-Ni^{II} complexes of Journaux and Garcia (0.12 V)[21,24] and other Ni^{II} complexes of the ligands with two $N_{amidate}$ atoms in conjunction with either two pyrrolidine (0.61 V),[20] two acetato (0.52 V),[21b] two amine groups in macrocyclic ligands and their open-chain analogues (0.495–0.580 V),[12a,12c] two phenolato (0.13 V),[25] two thiophenolato (–0.04 V)[25] and two thiolato (–0.24 to –0.42 V) groups.[25–26] The E_1 potential is, however, comparable to the ligands where two $N_{amidate}$ atoms are present in conjunction with two pyridine[20] (0.70 V), two 1-pyrroline[20] (0.71 V) and two amine groups in a 13-membered macrocyclic ligand (0.75–0.79 V).[12a,13c] This comparison indicates that the $Ni^{III/II}$ potential is quite sensitive to the variety of terminal donor groups used along with two $N_{amidate}$ donors. The potentials are typically more negative for the ligands capable of providing a tetraanionic coordination environment rather than a dianionic one about the nickel ion. The presence of a central phenylene bridge (as in **2**–**4**) has made the reduction potential more positive due to the delocalization of the negative charge on the deprotonated amide groups into the benzene ring.[21,24,27] This is in contrast to the cases where the bridge between two $N_{amidate}$ atoms is an ethylene unit (as in **1**) or a cyclohexane ring.[20]

Interestingly, a reversible reduction process (ΔE_p = 70 mV; i_{pc}/i_{pa} = 0.95–1.0) was also observed in the potential range from –1.67 to –1.86 V in CH_3CN for complexes **2**–**4** (Figure 8). Similar responses were observed when CV studies were performed in DMF. We assign these reductive process (E_R) to be nickel-centred on the basis of the similar observation for the square-planar Ni^{II} complexes of tetradentate amide-based ligands with E_R values ranging from –1.80 to –2.40 V.[20,28] Moreover, the significant shift in the E_R potential of complexes **2**–**4** towards more positive values according to **2** > **3** > **4** clearly indicates that the reduction process is metal-centred, which leads to a Ni^{I} species (Figure 8). This observed shift towards positive potential is consistent with the pronounced ligand field effect. If the site of reduction was ligand then the E_R potential would have come in a narrow range. It is important to mention that the macrocyclic Ni^{II} complexes do not show any reductive response in MeCN or DMF.[14] We speculate that the reduction is accompanied by a conformational change that is not supported by the rigid macrocyclic ligand framework in complexes **5**–**8**.

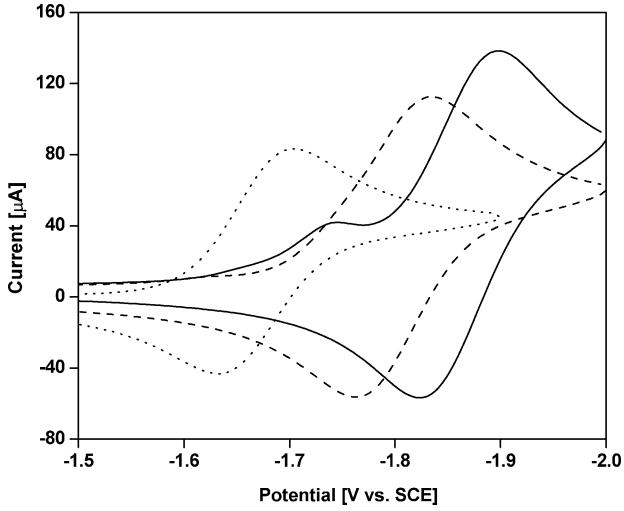

Figure 8. Cyclic voltammograms of complexes **2** (——), **3** (----) and **4** (...) in CH_3CN. The feature at –1.75 V for complex **2** is due to some impurity.

Coulometric oxidation at the E_1 and E_2 potentials for complexes **2**–**4** did not result in any observable colour change. For complex **1**, however, the original yellow colour changed to greenish-brown after oxidation at the E_1 poten-

tial; the resultant species decomposed immediately. A possible explanation is the unfavourable effect of the excess amount of supporting electrolyte present during the electrochemical oxidation.[29]

Electrochemistry in DMF

CVs were also recorded in DMF to see the effect of a better-coordinating and a more-polar solvent. A comparative CV plot is presented in Figure S8. Only complex **1** showed the quasireversible response with an E_1 value of 0.65 V (ΔE_p = 90 mV), whereas the other three complexes displayed only the irreversible responses with an E_{pa} value of ca. 0.8 V (Table 3). On comparison, the Ni^{III} state is better stabilized by ca. 0.1 V in DMF than in CH_3CN for complexes **1** and **2**. This could be due to the enhanced solvation as the polarity of the medium increased. The other two complexes, however, did not show any appreciable change in the E_1 potential, possibly due to the hindered accessibility of the solvent towards nickel ions as a result of the steric crowding. In fact, the crystal structure of **4** shows long-range cation···π and M···H bond interactions (vide supra) and supports this hypothesis.

Chemical Oxidation with $Cu(OTf)_2$

On the basis of the electrochemical findings, we attempted chemical oxidation of the present Ni^{II} complexes by using $Cu(OTf)_2$.[30] Our recent success to generate the Ni^{III} species of macrocyclic complexes **5**–**8**[14] and the redox potential of $Cu(OTf)_2$ (0.8 V in CH_3CN)[31] depicted its suitability. The addition of $Cu(OTf)_2$ (1 equiv.) to a CH_3CN solution of **1** immediately resulted in a colour change from deep-yellow to brownish-green, and new spectral features were observed at ca. 970 (ε = 200 $M^{-1}cm^{-1}$) and 635 nm (ε = 300 $M^{-1}cm^{-1}$) (Figure 9). These features are quite similar to those of its macrocyclic analogue $[\mathbf{5}^{Ox}]^+$ and point towards a similar electronic chromophore.[14] This species, however, is not very stable and decomposes to product(s) of unassignable nature. Complex **2** also afforded a greenish-brown species after its treatment with $Cu(OTf)_2$. The absorption spectrum of this new species, $[\mathbf{2}^{Ox}]^+$, showed features at 1020, 890, 790, ca. 700 and 480 nm with the ε value between 200–500 $M^{-1}cm^{-1}$ (Figure 9). The observed absorption spectral features of $[\mathbf{2}^{Ox}]^+$ have some similarity with the macrocyclic systems $[\mathbf{7}^{Ox}]^+$ and $[\mathbf{8}^{Ox}]^+$ and again suggests a similar electronic chromophore.[14] The solution-generated $[\mathbf{1}^{Ox}]^+$ also displayed anisotropic signals in the X-band EPR spectrum at 77 K with g values of 2.278, 2.232 and 2.009 (Figure 10). The corresponding values for $[\mathbf{2}^{Ox}]^+$ species are 2.300, 2.230 and 2.015. The EPR spectra of $[\mathbf{1}^{Ox}]^+$ and $[\mathbf{2}^{Ox}]^+$ are very similar to the macrocyclic systems $[\mathbf{5}^{Ox}]^+$ – $[\mathbf{8}^{Ox}]^+$, which thus suggests a Ni^{III} ion in a square-planar environment.[14] The large rhombicity and a high average g value of ca. 2.17 suggests that the locus of the oxidation is nickel centre as also concluded with macrocyclic systems[14] $[\mathbf{5}^{Ox}]^+$ – $[\mathbf{8}^{Ox}]^+$ and other literature precedents.[21,24,27] Complexes **3** and **4** did not show any change upon treatment with $Cu(OTf)_2$ (1 equiv.), whereas decomposition occurred when an excess amount of the oxidant (≥3 equiv.) was used.

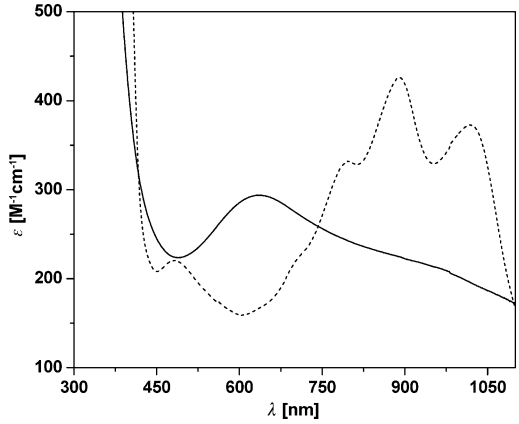

Figure 9. Absorption spectra of $[\mathbf{1}^{Ox}]^+$ (——) and $[\mathbf{2}^{Ox}]^+$ (– – –) in CH_3CN after oxidation of **1** and **2** with $Cu(OTf)_2$.

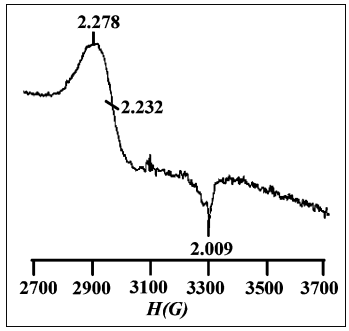

Figure 10. EPR spectrum of $[\mathbf{1}^{Ox}]^+$ in CH_3CN at 77 K after oxidation with $Cu(OTf)_2$.

Preliminary Epoxidation Reactions

The chemical oxidation [with $Cu(OTf)_2$] of complexes **1** and **2**, which resulted in the generation of a metastable Ni^{III} species, suggested that other complexes may also transiently stabilize the higher oxidation state of the nickel ion. It was suggested that the diamagnetic square-planar Ni^{II} complexes with an accessible Ni^{III} oxidation state display oxidation activities.[32] This prompted us to probe possible substrate oxidation reactions. Ni^{II} complexes **1**–**4** were tested as catalysts for the epoxidation of alkenes in the presence of aldehyde [$(CH_3)_3CHO$ or $(CH_3)_2CH_2CHO$] as coreductor and dioxygen as the oxidizing agent.[33] All catalytic reactions were carried out in MeCN and the results are summarized in Table 4. This type of transformation is considered to occur via high-valent metal-oxido intermediates;[34] however, a radical pathway was also suggested in many cases.[35] Addition of the aldehyde to an aerated solution of the nickel complex resulted in distinct colour change. It is to be noted, however, that no colour change (and apparently generation of the active species) was noticed by the reaction between aldehyde and Ni^{II} complexes under inert atmo-

sphere. This experiment rules out the possibility of the generation of the acyl radical (RC·O) by the direct reaction between the Ni^{II} complexes and aldehyde as commonly suggested.[34] We believe that the reaction between the Ni^{II} complex with aldehyde and O_2 concomitantly produces the *reactive* Ni^{x+}*–O species* and the acid. Typically, the colour changed from yellow to greenish-brown after the addition of the aldehyde and O_2 to the solution of **1**, **2** and **4** was accompanied with distinct features in the absorption spectra. Complex **3**, however, immediately decomposed. This trend also supports the observed reactivity pattern of various substrates with the catalysts. Complex **1** was found to be the most effective catalyst amongst all complexes with the following trend: **1** > **2** > **4**. The introduction of the electron-withdrawing group in the *para* position of the phenyl group in styrene resulted in reduced epoxidation as observed before[35a] (Table 4, Entries 15–18). For example, the turn over number (TON) was reduced from 460 to 210 after the introduction of the Cl group in the *para* position (Table 4, compare Entries 10 and 15). For the *cis*-stilbene epoxidation reaction, *trans*-stilbene oxide was the only product,[34b,35a] which thus suggests the free rotation of the C–C bond in the transition state for an asynchron C–O bond formation. As anticipated, the percent conversion as well as the TON for the *trans*-stilbene epoxidation reaction were much higher than *cis*-stilbene (Table 4, Entries 1–4 and 5–9), as the step corresponding to the rotation of the C–C bond was not required. Catalyst **4** was found to efficiently epoxidize *trans*-stilbene with 97% conversion and a TON of 285, whereas it was moderate with other substrates. We believe that the appended benzyl substituents help to bring the *trans*-stilbene closer to the nickel centre through π–π interactions. In fact, the crystal structure of **4** shows long-range interactions and supports this hypothesis.

Other oxidants, such as, PhIO, *tert*-butylhydroperoxide, *m*-chloroperbenzoic acid, H_2O_2 and urea·H_2O_2 adduct were also used to understand the nature of the oxidizing agent in the epoxidation reaction. However, only *tert*-butylhydroperoxide was found to cause epoxidation of the *trans*-stilbene with ca. 15% conversion. The conversion increased to ca. 20% when the epoxidation reaction was carried out under a O_2 atmosphere.[35,36] This suggests that a radical pathway might be involved in the aerobic epoxidation reaction with *tert*-butylhydroperoxide. However, the high yield of the epoxide products observed for the aldehyde–O_2 combination reactions strongly suggest the involvement of the Ni complexes in the epoxidation reaction.

Table 4. Summary of the Ni^{II} complex catalyzed oxidation of alkenes.[a]

Entry	Substrate	Complex	% Conversion [e]	TON[f]
1	*cis*-stilbene	**1**	40	21
2	*cis*-stilbene	**2**	38	20
3	*cis*-stilbene	**3**	56	30
4	*cis*-stilbene	**4**	35	19
5[b]	*trans*-stilbene	**1**	50	400
6[c]	*trans*-stilbene	**1**	100	285
7	*trans*-stilbene	**2**	52	29
8	*trans*-stilbene	**3**	13	6
9[c]	*trans*-stilbene	**4**	97	285
10[b]	styrene	**1**	55	460
11[c]	styrene	**1**	100	285
12[d]	styrene	**2**	93	134
13	styrene	**3**	NR	NR
14	styrene	**4**	55	32
15[c]	*p*-chlorostyrene	**1**	78	210
16[c]	*p*-chlorostyrene	**2**	54	144
17	*p*-chlorostyrene	**3**	NR	NR
18	*p*-chlorostyrene	**4**	96	54

[a] Catalyst: 1.66 mol-% (1 mmol), isobutyraldehyde (180 mmol), substrate (60 mmol), solvent: CH_3CN, reaction time: 45 min. [b] Catalyst: 0.1 mol-% (1 mmol), isobutyraldehyde (3000 mmol), substrate (1000 mmol). [c] Catalyst: 0.33 mol-% (1 mmol), isobutyraldehyde (900 mmol), substrate (300 mmol). [d] Catalyst: 0.66 mol-% (1 mmol), isobutyraldehyde (450 mmol), substrate (150 mmol). [e] %Conversion = amount of substrate consumed × 100/amount of initial substrate. [f]. TON = Turn over number; NR = No reaction.

Conclusions

We show the synthesis and characterization of four square-planar nickel(II) complexes with open-chain amide-based ligands. The crystal structure analysis of **2** and **4** substantiate the square-planar geometry around the Ni^{II} ion. In addition, complex **4** also shows long-range cation–π interactions from the benzyl substituents, which thus creates a pseudooctahedral geometry around the metal ion. Other weak interactions (H-bonding, C–H···X and π–π) generate an interesting structural pattern for complex **4**. The electrochemical results suggest that the Ni^{III}/Ni^{II} redox couple primarily depends upon the N_4 donors composed of two N_{amide} and two N_{amine} atoms and not on the peripheral substituents. All four ligands with variable backbone and substituents are equally competent in stabilizing the Ni^{III} state. This is in contrast with the macrocyclic complexes **5**–**8**, where a pronounced ligand field effect was observed for the Ni^{III}/Ni^{II} redox couple. Whereas the electrochemical oxidation of **5**–**8** generated the respective Ni^{III} species in the macrocyclic systems, complexes **1**–**4** were found completely unresponsive. Chemical oxidation of **1** and **2** with Cu(OTf)$_2$, however, transiently generated the Ni^{III} species, which was characterized by absorption and EPR spectral studies. These spectral studies indicate that $[\mathbf{1}^{Ox}]^+$ and $[\mathbf{2}^{Ox}]^+$ are quite similar to the macrocyclic systems $[\mathbf{5}^{Ox}]^+$ – $[\mathbf{8}^{Ox}]^+$, in which the Ni^{III} ion is in a square-planar geometry. Epoxidation of the alkenes with O_2–aldehyde combination suggests that the present nickel complexes have the ability to transiently stabilize the higher oxidation state of the nickel ion that possibly participates in the substrate oxidation.

Experimental Section

Materials and Reagents: All reagents were obtained from commercial sources and used as received. *N*, *N*-dimethylformamide (DMF) was dried and distilled from 4 Å molecular sieves and stored over sieves. Acetonitrile (MeCN) was dried by distillation from anhy-

drous CaH_2. Diethyl ether was dried by refluxing over sodium metal under an inert atmosphere. Tetrahydrofuran (THF) was dried by refluxing and distilling from sodium metal and benzophenone. Ethyl alcohol (C_2H_5OH) and methyl alcohol (CH_3OH) were distilled from magnesium ethoxide and magnesium methoxide, respectively. Chloroform ($CHCl_3$) and dichloromethane (CH_2Cl_2) were purified by washing with 5% sodium carbonate solution followed by water and finally dried with anhydrous $CaCl_2$ before a final reflux and distillation. The compounds *N*, *N*′-bis(chloroacetyl)ethylenediamine and *N*,*N*′-bis(chloroacetyl)-*o*-phenylenediamine were prepared as reported earlier,[14] whereas the ligand H_2L^2 was synthesized as described recently.[22]

Ligand Synthesis

H_2L^1: To a solution of *N*, *N*′-bis(chloroacetyl)ethylenediamine (2.0 g, 9.38 mmol) in ethyl alcohol (25 mL) was added aqueous dimethylamine (40%, 6.8 g, 56.33 mmol). The resulting mixture was heated at reflux for 24 h. The solvent was removed under reduced pressure, followed by the addition of a saturated aqueous solution (10 mL) of sodium hydrogen carbonate to the oil. The resultant mixture was extracted with CH_2Cl_2 (3 × 10 mL). The CH_2Cl_2 layers were combined and dried with anhydrous Na_2SO_4. The filtrate was evaporated under reduced pressure to afford a white solid. Yield: 1.5 g (62%). M.p. 98–100 °C. ^{1}H NMR (300 MHz, $CDCl_3$, 25 °C): δ = 2.2 (s, 12 H, CH_3), 2.9 [s, 4 H, -CH_2C(O)-], 3.4 (s, 4 H, -CH_2-CH_2), 7.4 (br. s, 2 H, NH) ppm. IR (KBr, selected peaks): $\tilde{\nu}$ = 3288 ν(NH), 2944, 2820, 2772 ν(CH), 1656 ν(CO) cm^{-1}. MS (CH_3CN): *m*/*z* = 230.8 [M + H]$^+$. $C_{10}H_{22}N_4O_2$·0.5H_2O (239.3): calcd. C 50.14, H 9.6, N 23.14; found C 50.29, H 9.25, N 23.64.

H_2L^3: This ligand was synthesized in a similar manner to that used for H_2L^1 with the following reagents: *N*,*N*′-bis(chloroacetyl)-*o*-phenylenediamine (2.0 g, 7.66 mmol) and diethylamine (3.38 g, 45.97 mmol). The filtrate was evaporated under reduced pressure to afford a yellow semisolid. Yield: 2.2 g (86%). ^{1}H NMR (300 MHz, $CDCl_3$, 25 °C): δ = 1.09 (t, *J* = 7.1 Hz, 12 H, CH_3), 2.65 (q, *J* = 7.1 Hz, 8 H, -CH_2-CH_3), 3.18 [s, 4 H, -CH_2C(O)-], 7.20 (m, 2 H, aromatic-H), 7.59 (m, 2 H, aromatic-H), 9.4 (br. s, 2 H, NH) ppm. IR (KBr, selected peaks): $\tilde{\nu}$ = 3244 ν(NH), 2970 ν(CH), 1683 ν(CO), 1596 ν(C=C) cm^{-1}. MS (CH_3CN): *m*/*z* = 335.5 [M + H]$^+$. $C_{18}H_{30}N_4O_2$ (334.5): calcd. C 64.67, H 8.98, N 16.76; found C 64.78, H 9.20, N 16.73.

H_2L^4: This ligand was synthesized in a similar manner to that for H_2L^1 with the following reagents: *N*,*N*′-bis(chloroacetyl)-*o*-phenylenediamine (2.0 g, 7.66 mmol) and dibenzylamine (9.06 g, 45.97 mmol). Yield: 4.24 g (95%). M.p. 150–152 °C. ^{1}H NMR (300 MHz, $CDCl_3$, 25 °C): δ = 3.20 [s, 4 H, -CH_2C(O)-], 3.60 (s, 8 H, -CH_2Ph), 7.17 (m, 2 H, aromatic-H), 7.29 (m, 20 H, Ph- H), 7.46 (m, 2 H, aromatic-H), 9.27 (br. s, 2 H, NH) ppm. IR (KBr, selected peaks): $\tilde{\nu}$ = 3278 ν(NH), 3060, 3025, 2811 ν(CH), 1663 ν(CO), 1594 ν(C=C) cm^{-1}. MS (CH_3CN): *m*/*z* = 584.3 [M + H]$^+$. $C_{38}H_{38}N_4O_2$ (582.8): calcd. C 78.35, H 6.52, N 9.22; found C 78.31, H 7.00, N 9.22.

Synthesis of Nickel Complexes

[Ni(L^1)]·1.5H_2O (1): The H_2L^1 ligand (0.20 g, 0.86 mmol) was dissolved in DMF (5 mL) and treated with NaH (0.046 g, 1.92 mmol) under a nitrogen atmosphere. The mixture was stirred until H_2 evolution ceased (ca. 15–20 min). To this mixture was added a solution of $NiCl_2$ (0.112 g, 0.86 mmol) in DMF (8 mL) under inert conditions. The resulting mixture was further stirred for 2 h at room temperature, which resulted in an orange solution. This solution was filtered through a pad of Celite atop a medium-porosity frit. The filtrate was concentrated under reduced pressure to one quarter of its original volume, and diethyl ether was added to precipitate the crude product as deep-orange powder. The recrystallization was achieved by diffusing diethyl ether into a CH_2Cl_2 solution of the crude product at room temperature. Yield: 0.20 g (82%). ^{1}H NMR (300 MHz, [D_6]DMSO, 25 °C): δ = 2.52 (s, 12 H, -CH_3), 2.69 [s, 4 H, -CH_2C(O)-], 2.94 (s, 4 H, -CH_2-CH_2-) ppm. ^{13}C NMR (75 MHz, [D_6]DMSO, 25 °C): δ = 46 (-CH_3), 50 (-CH_2CH_2-), 70 [-C(O)CH_2-], 172 (C=O) ppm. FTIR (KBr disk): $\tilde{\nu}$ = 3375, 3207, 2950, 2923, 2849, 1614 cm^{-1}. Conductivity (CH_3CN, ca. 1 mM solution, 298 K): Λ_M = 4 Ω^{-1} cm^{2}mol^{-1}. UV/Vis (CH_3CN): λ_{max} (ε, M^{-1}cm^{-1}) = 515 sh. (90), 435 (410), 264 sh. (6300), 240 sh. (11700) nm. UV/Vis (DMF): λ_{max} (ε, M^{-1}cm^{-1}) = 518 sh. (50), 435 (280) nm. UV/Vis (DMSO): λ_{max} (ε, M^{-1}cm^{-1}) = 518 sh. (50), 435 (280) nm. UV/Vis (H_2O): λ_{max} (ε, M^{-1}cm^{-1}) = 435 (100) nm. MS (EI+, CH_3CN): *m*/*z* = 287.08 [M + H]$^+$. $C_{10}H_{20}N_4O_2Ni$·1.5H_2O (313.69): calcd. C 38.28, H 7.33, N 17.85; found C 38.27, H 7.83, N 17.56.

[Ni(L^2)] (2): This compound was synthesized in a similar fashion to that used for **1**. However, the filtrate was directly subjected to the diethyl ether diffusion to afford an orange-coloured, highly crystalline product in 70% yield. ^{1}H NMR (300 MHz, $CDCl_3$, 25 °C): δ = 2.63 (s, 12 H, -CH_3), 3.26 [s, 4 H, -CH_2C(O)-], 6.76 (m, 2 H, Ar-1a), 8.26 (m, 2 H, Ar-1b) ppm. ^{1}H NMR (300 MHz, [D_6]-DMSO, 25 °C): δ = 2.63 (s, 12 H, -CH_3), 3.17 [s, 4 H, -CH_2C(O)-], 6.57 (m, 2 H, Ar-1a), 8.05 (m, 2 H, Ar-1b) ppm. ^{13}C NMR (75 MHz, [D_6]DMSO, 25 °C): δ = 50 (-CH_3), 70 [-C(O)CH_2-],120 (-CH, Ar-1a), 122 (-CH, Ar-1b), 142 (Ar-1c), 172 (C=O) ppm. FTIR (KBr disk): $\tilde{\nu}$ = 3051, 3003, 2920, 1636, 1572 cm^{-1}. Conductivity (CH_3CN, ca. 1 mM solution, 298 K): Λ_M = 5 Ω^{-1} cm^{2}mol^{-1}. UV/Vis (CH_3CN): λ_{max} (ε, M^{-1}cm^{-1}) = 540 sh. (60), 445 (280), 360 sh. (110), 293 (13500), 268 (17800) nm. UV/Vis (DMF): λ_{max} (ε, M^{-1}cm^{-1}) = 540 sh. (50), 445 (250), 355 sh. (120), 296 (16500) nm. UV/Vis (DMSO): λ_{max} (ε, M^{-1}cm^{-1}) = 530 sh. (60), 446 (330) nm. UV/Vis (H_2O): λ_{max} (ε, M^{-1}cm^{-1}) = 449 (310) nm. MS (EI+, CH_3OH): *m*/*z* = 357.69 [M + Na]$^+$. $C_{14}H_{20}N_4NiO_2$ (334.3): calcd. C 50.19, H 5.9, N 16.73; found C 50.15, H 5.85, N 16.48.

[Ni(L^3)] (3): This compound was synthesized in a similar fashion to that used for **1**. The recrystallized complex was isolated in 80% yield as deep-orange blocks after diffusing diethyl ether into a dichloromethane solution. ^{1}H NMR (300 MHz, [D_6]DMSO, 25 °C): δ = 1.87 (t, *J* = 7 Hz, 12 H, -CH_3), 2.45 (m, 4 H, -CH_2-3a), 2.92 (m, 4 H, -CH_2-3b), 3.16 [s, 4 H, -CH_2C(O)-], 6.56 (m, 2 H, Ar-1a), 8.15 (m, 2 H, Ar-1b) ppm. ^{1}H NMR (300 MHz, $CDCl_3$, 25 °C): δ = 1.99 (s, 12 H, -CH_3), 2.45 (q, *J* = 6 Hz, 4 H, -CH_2-3a), 2.84 (q, *J* = 6 Hz, 4 H, -CH_2-3b), 3.18 [s, 4 H, -CH_2C(O)-], 6.74 (m, 2 H, Ar-1a), 8.30 (m, 2 H, Ar-1b) ppm. ^{13}C NMR (75 MHz, $CDCl_3$, 25 °C): δ = 12 (-CH_3), 55 (-CH_2-CH_3), 65 [-C(O)CH_2-], 119 (-CH, Ar-1a), 121 (-CH, Ar-1b), 142 (Ar-1c), 173 (C=O) ppm. FTIR (KBr disk): $\tilde{\nu}$ = 3058, 3001, 2968, 1625, 1566 cm^{-1}. Conductivity (CH_3CN, ca. 1 mM solution, 298 K): Λ_M = 5 Ω^{-1} cm^{2}mol^{-1}. UV/Vis (CH_3CN): λ_{max} (ε, M^{-1}cm^{-1}) = 570 sh. (40), 460 (280), 370 sh. (90), 300 sh. (8500), 290 sh. (9800), 270 (17000), 220 (36600) nm. UV/Vis (DMF): λ_{max} (ε, M^{-1}cm^{-1}) = 565 sh. (60), 460 (360), 374 sh. (120), 308 sh. (12000), 295 sh. (12900). UV/Vis (DMSO): λ_{max} (ε, M^{-1}cm^{-1}) = 564 sh. (40), 460 (311), 370 sh. (90). UV/Vis (H_2O): λ_{max} (ε, M^{-1}cm^{-1}) = 464 (340). MS (EI+, CH_3OH): *m*/*z* = 392.8 [M + H]$^+$. $C_{18}H_{28}N_4NiO_2$ (391.15): calcd. C 55.22, H 7.16, N 14.33; found C 55.08, H 7.50, N 14.11.

[Ni(L^4)]·H_2O (4): This compound was synthesized in a similar fashion to that used for **1**. Instead of $NiCl_2$, $(Et_4N)_2[NiCl_4]$ was used. The crude complex was recrystallized by diffusing diethyl ether into a MeCN solution to afford the product in 48% yield. ^{1}H NMR (300 MHz, [D_6]DMSO, 25 °C): δ = 2.50 [s, 4 H, -CH_2C(O)-], 2.58

(d, J = 12 Hz, 4 H, -CH_2-3a), 3.65 (d, J = 12 Hz, 4 H, -CH_2-3b), 6.65 (m, 2 H, Ar-1a), 7.63 (s, 12 H, Ar-5&6), 8.11 (m, 2 H, Ar-1b), 8.14 (s, 8 H, Ar-4) ppm. ^{13}C NMR (75 MHz, [D_6]DMSO, 25 °C): δ = 58 (-CH_2-4), 65 [-C(O)CH_2-], 119 (-CH, Ar-1a), 121 (-CH, Ar-1b), 129 (-CH, Ar-7&8), 133 (Ar-5&6), 142 (Ar-1c), 170 (C=O) ppm. FTIR (KBr disk): $\tilde{\nu}$ = 3430, 3033, 2931, 1622, 1569 cm^{-1}. Conductivity (CH_3CN, ca. 1 mM solution, 298 K): Λ_M = 5 Ω^{-1} cm^2 mol^{-1}. UV/Vis (CH_3CN): λ_{max} (ε, M^{-1} cm^{-1}) = 540 sh. (190), 470 (420), 397 sh. (220), 310 sh. (12000), 270 (25000). UV/Vis (DMF): λ_{max} (ε, M^{-1} cm^{-1}) = 550 sh. (170), 470 (400), 385 sh. (200), 311 sh. (11700). UV/Vis (DMSO): λ_{max} (ε, M^{-1} cm^{-1}) = 550 sh. (120), 470 (300), 387 sh. (140). MS (EI+, CH_3OH): m/z = 639.76 $[M + H]^+$. $C_{38}H_{36}N_4NiO_2 \cdot H_2O$ (657.41): calcd. C 69.37, H 5.78, N 8.52; found C 69.12, H 6.12, N 8.28.

General Procedure for the Epoxidation Reaction: To a solution of the Ni^{II} complex (0.1–1.66 mol-%) in CH_3CN (10 mL) was added isobutyraldehyde (180–3000 mmol) and the substrate (60–1000 mmol). The reaction mixture was stirred at room temperature under an O_2 atmosphere for 45 min. The progress of the reaction was monitored by thin-layer chromatography ($CHCl_3$/hexanes, 1:1). The solvent was removed under reduced pressure, and the oxidation products were separated and purified by column chromatography on silica gel ($CHCl_3$/hexanes, 1:1).

Physical Measurements: The conductivity measurements were done in organic solvents by using the digital conductivity bridge from the Popular Traders, India (model number: PT – 825). The elemental analysis data were obtained with an Elementar Analysen Systeme GmbH Vario EL-III instrument. The NMR measurements were done with either a Hitachi R-600 FT NMR (60 MHz) or an Avance Bruker (300 MHz) instrument. The infrared spectra (either as KBr pellet or as a mull in mineral oil) were recorded with a Perkin–Elmer FTIR 2000 spectrometer. The absorption spectra were recorded with a Perkin–Elmer Lambda 25 spectrophotometer. The mass spectra were obtained with a Jeol SX102/DA–6000 instrument.

Electrochemical Measurements: Cyclic voltammetric experiments were performed by using a PAR model 370 electrochemistry system consisting of an M-174A polarographic analyzer, M-175 universal programmer and RE 0074 X-Y recorder or a CH Instruments electrochemical analyzer (600B Series). The cell contained a glassy-carbon (PAR model G0021) or a Beckman Pt (M-39273) working electrode, a Pt wire auxiliary electrode and a saturated calomel electrode (SCE) as the reference electrode. A salt bridge (containing supporting electrolyte, TBAP, dissolved in either MeCN or DMF) was used to connect the SCE with the experimental solution.[37] For constant potential electrolysis experiments a Pt mesh was used as the working electrode. The solutions were ca. 1 mM in complex and ca. 0.1 M in supporting electrolyte, TBAP. Under our experimental conditions, the $E_{1/2}$ values (in Volts) for the couple Fc^+/Fc were 0.40 in MeCN vs. SCE.

Crystal Structure Determination: Single crystals suitable for X-ray diffraction studies were grown by the vapour diffusion of diethyl ether into either a DMF solution (for **2**) or CH_3CN solution (for **4**). For complex **2**, X-ray diffraction studies of crystal mounted on a capillary were carried out with a Bruker AXS SMART-APEX diffractometer with a CCD area detector (K_α = 0.71073 Å, monochromator: graphite).[38] Frames were collected at T = 293 K by ω, <?oασ [oo?>ϕ<?oασ [oξ?> and 2θ-rotation at 10 s per frame with SAINT.[39] The measured intensities were reduced to F^2 and corrected for absorption with SADABS.[40] Structure solution, refinement and data output were carried out with the SHELXTL program.[40] A total of 2580 reflections were measured, of which 2336 reflections [$I > 2\sigma(I)$] were used in the structure refinement. Non-hydrogen atoms were refined anisotropically. All hydrogen atoms were placed in geometrically calculated positions by using a riding model. For **4**, the intensity data were collected at 295 K with a Siemens P4 X-ray diffractometer by using θ–2θ scanning mode with graphite monochromated Mo-K_α radiation. A total of 6835 reflections were measured, of which 6446 were unique and 3278 were considered observed [$I > 2\sigma(I)$]. The data were corrected for Lorentz and polarization effects and a psi-scan absorption correction was also applied. The structure was solved by direct methods and refined by full-matrix least-squares refinement techniques on F^2. All non-hydrogen atoms were refined anisotropically. All hydrogen atoms were attached with Uiso values of 1.2 times (for methylene and phenylene carbon atoms) and 1.5 times (methyl carbon atoms) the Uiso values of their respective carrier atoms. Details of the crystallographic data are given in Table 5.

Table 5. Crystallographic data for [Ni(L^2)] (**2**) and [Ni(L^4)]·CH_3CN (**4**).

	[Ni(L^2)] (**2**)	[Ni(L^4)]·CH_3CN (**4**)
Empirical formula	$C_{14}H_{20}N_4O_2Ni$	$C_{40}H_{39}N_5O_2Ni$
Formula mass	335.05	680.48
T [K]	298(2)	295(2)
Crystal system	triclinic	triclinic
Space group	$P\bar{1}$	$P\bar{1}$
Colour, shape	orange, block	brown, needle
Size [mm]	0.2 × 0.1 × 0.2	0.18 × 0.16 × 0.16
a [Å]	8.974(2)	10.293(3)
b [Å]	9.612(3)	11.109(3)
c [Å]	9.688(3)	16.194(4)
α [°]	112.655(4)	95.62(2)
β [°]	91.538(4)	107.25(2)
γ [°]	105.001(4)	97.82(2)
V [Å^3]	737.4(4)	1733.2(8)
Z	2	2
F [000]	352	716
$D_{calcd.}$ [g cm^{-3}]	1.509	1.304
Absorption coeff. [mm^{-1}]	1.325	0.602
R[a]		
R_w[b]	0.0383	0.0549
GOF on F^2	0.0877	0.1247
	1.084	0.834

[a] $R = \Sigma||F_o| - |F_c||/\Sigma|F_o|$. [b] $R_w = \{[\Sigma(|F_o|^2|F_c|^2)^2]\}^{1/2}$.

CCDC-663277 (for **2**) and -663278 (for **4**) contain the supplementary crystallographic data for this paper. These data can be obtained free of charge from The Cambridge Data Centre via www.ccdc.cam.ac.uk/data_request/cif.

Supporting Information (see footnote on the first page of this article): Crystal structure of complex **4**; absorption spectra for complexes **1**–**4** recorded in DMF and DMSO; ^{1}H and ^{13}C NMR spectra for complexes **1**–**4** recorded in [D_6]DMSO; cyclic voltammograms; H-bonding distances for complex **4**.

Acknowledgments

R. G. thanks University Grant Commission (UGC), Department of Science & Technology (DST) both Government of India, New Delhi, for generous financial support, DST-FIST-funded single-

crystal diffraction facility at IIT-Delhi for the data collection of complex **2** and MS facility at this department for the mass spectra. We sincerely thank Professor R. Mukherjee and his research group at IIT–Kanpur for helping us with electrochemical experiments. J. S. thanks UGC for a fellowship (SRF).

[1] a) J. R. Lancaster Jr, in *The Bioinorganic Chemistry of Nickel*, VCH, New York, **1988**; b) S. B. Mulrooney, R. P. Hausinger, *FEMS Microbiol. Rev.* **2003**, *27*, 239.

[2] a) R. Cammack, *Adv. Inorg. Chem.* **1988**, *32*, 297; b) J. J. G. Moura, I. Moura, M. Teixeira, A. V. Xavier, G. D. Fauque, J. Legall, *Met. Ions Biol. Syst.* **1988**, *23*, 285; c) H.-D. Youn, E.-J. Kim, J.-H. Roe, Y. C. Hah, S.-O. Kang, *Biochem. J.* **1996**, *318*, 889; d) P. A. Lindahl, *Biochemistry* **2002**, *41*, 2097; e) U. Ermler, W. Grabarse, S. Shima, M. Goubeaud, R. K. Thauer, *Science* **1997**, *278*, 1457.

[3] a) J. D. Koola, J. K. Kochi, *Inorg. Chem.* **1987**, *26*, 908; b) H. Yoon, C. J. Burrows, *J. Am. Chem. Soc.* **1988**, *110*, 4087; c) T. R. Wagler, C. J. Burrows, *Tetrahedron Lett.* **1988**, *29*, 5091; d) B. Dangel, M. Clarke, J. Haley, D. Sames, R. Polt, *J. Am. Chem. Soc.* **1997**, *119*, 10865; e) T. R. Wagler, Y. Fang, C. J. Burrows, *J. Org. Chem.* **1989**, *54*, 1584.

[4] a) V. M. Fernandez, E. C. Hatchikian, D. S. Patil, R. Cammack, *Biochem. Biophys. Acta* **1996**, *883*, 415; b) A. Volbeda, M. H. Charco, C. Piras, E. C. Hatchikian, M. Frey, J. C. Fontecilla-Camps, *Nature* **1995**, *373*, 580; c) J. C. Fontecella-Camps, S. W. Ragsdale, *Adv. Inorg. Chem.* **1999**, *47*, 283; d) M. J. Maroney, P. A. Bryngelson, *J. Biol. Inorg. Chem.* **2001**, *6*, 453.

[5] a) S. B. Choudhury, J. W. Lee, G. Davidson, Y. I. Yim, K. Bose, M. L. Sharma, S. O. Kang, D. E. Cabelli, M. J. Maroney, *Biochemistry* **1999**, *38*, 3744; b) R. Cammack, P. Vliet in *Bioinorganic Catalysis* (Ed.: J. Reedijk), Marcel Dekkar, New York, **1999**.

[6] a) S. W. Ragsdale, M. Kumar, *Chem. Rev.* **1996**, *96*, 2515; b) C. G. Riordan, *J. Biol. Inorg. Chem.* **2004**, *9*, 509; c) C. L. Drennan, T. I. Doukov, S. W. Ragsdale, *J. Biol. Inorg. Chem.* **2004**, *9*, 511; d) A. Volbeda, J. C. Fontecilla-Camps, *J. Biol. Inorg. Chem.* **2004**, *9*, 525.

[7] a) P. A. Lindahl, *J. Biol. Inorg. Chem.* **2004**, *9*, 516; b) T. C. Brunold, *J. Biol. Inorg. Chem.* **2004**, *9*, 533; c) C. G. Riordan, *J. Biol. Inorg. Chem.* **2004**, *9*, 542.

[8] I. Zilbermann, E. Maimon, H. Cohen, D. Meyerstein, *Chem. Rev.* **2005**, *105*, 2609.

[9] A. L. Gavrilova, B. Bosnich, *Chem. Rev.* **2004**, *104*, 349.

[10] a) M. Kodama, T. Yatsunami, E. Kimura, *J. Chem. Soc., Dalton Trans.* **1979**, 1783; b) M. Kodama, E. Kimura, *J. Chem. Soc., Dalton Trans.* **1981**, 694; c) E. Kimura, A. Sakonaka, R. Machida, M. Kodama, *J. Am. Chem. Soc.* **1982**, *104*, 4255; d) E. Kimura, T. Koike, R. Machida, R. Nagai, M. Kodama, *Inorg. Chem.* **1984**, *23*, 4181; e) X. H. Bu, D. L. An, X. C. Cao, Y. T. Chen, M. Shionoya, E. Kimura, *Polyhedron* **1996**, *15*, 161; f) X. H. Bu, X. C. Cao, Z. Z. Zhang, Z. A. Zhu, Y. T. Chen, M. Shionoya, E. Kimura, *Polyhedron* **1996**, *15*, 1203; g) X. H. Bu, D. L. An, Z. A. Zhu, Y. T. Chen, M. Shionoya, E. Kimura, *Polyhedron* **1997**, *16*, 179.

[11] a) E. Kimura, *J. Coord. Chem.* **1986**, *15*, 1 and references cited therein; b) T. Ito, M. Kato, M. Yamashita, H. Ito, *J. Coord. Chem.* **1986**, *15*, 29 and references cited therein.

[12] a) S. P. Gavrish, Y. D. Lampeka, P. Lightfoot, H. Pritzkow, *Dalton Trans.* **2007**, 4708; b) Y. D. Lampeka, S. P. Gavrish, R. W. Hay, T. Eisenblatter, P. Lightfoot, *J. Chem. Soc., Dalton Trans.* **2000**, 2023; c) S. P. Gavrish, Y. D. Lampeka, P. Lightfoot, *Inorg. Chim. Acta* **2004**, *357*, 1023.

[13] a) Y. D. Lampeka, S. P. Gavrish, *J. Coord. Chem.* **1990**, *21*, 351; b) S. P. Gavrish, Y. D. Lampeka, *J. Coord. Chem.* **1991**, *24*, 351; c) S. P. Gavrish, Y. D. Lampeka, *J. Coord. Chem.* **1996**, *38*, 295.

[14] S. K. Sharma, S. Upreti, R. Gupta, *Eur. J. Inorg. Chem.* **2007**, 3247.

[15] K. Nakamoto in *Infrared and Raman Spectra of Inorganic and Coordination Compounds*, John Wiley & Sons, **1986**.

[16] W. J. Geary, *Coord. Chem. Rev.* **1971**, *7*, 81.

[17] a) D. A. Dougherty, *Science* **1996**, *271*, 163; b) J. C. Ma, D. A. Dougherty, *Chem. Rev.* **1997**, *97*, 133.

[18] a) M. J. Calhorda, *Chem. Commun.* **2000**, 801; b) D. Braga, F. Grepioni, E. Tedesco, K. Biradha, G. R. Desiraju, *Organometallics* **1997**, *16*, 1846; c) C. E. MacBeth, P. L. Larsen, T. N. Sorrel, D. Powell, A. S. Borovik, *Inorg. Chim. Acta* **2002**, *341*, 77.

[19] a) M. Mulqi, F. S. Stephens, R. S. Vagg, *Inorg. Chim. Acta* **1981**, *52*, 73; b) F. S. Stephens, R. S. Vagg, *Inorg. Chim. Acta* **1982**, *57*, 9; c) F. S. Stephens, R. S. Vagg, *Inorg. Chim. Acta* **1984**, *90*, 17; d) F. S. Stephens, R. S. Vagg, *Inorg. Chim. Acta* **1986**, *120*, 165.

[20] C. L. Weeks, P. Turner, R. R. Fenton, P. A. Lay, *J. Chem. Soc., Dalton Trans.* **2002**, 931.

[21] a) A. Aukauloo, X. Ottenwaelder, R. Ruiz, S. Poussereau, Y. Pei, Y. Journaux, P. Fleurat, F. Volatron, B. Cervera, M. C. Munoz, *Eur. J. Inorg. Chem.* **1999**, 1067; b) X. Ottenwaelder, A. Aukauloo, Y. Journaux, R. Carrasco, J. Cano, B. Cervera, I. Castro, S. Curreli, M. C. Munoz, A. L. Rosello, B. Soto, R. Ruiz-Garcia, *Dalton Trans.* **2005**, 2516.

[22] J. Singh, G. Hundal, M. Corbella, R. Gupta, *Polyhedron* **2007**, *26*, 3893.

[23] The electrochemical feature at 0.82 V does not disappear or change with a change in solvent (CH_3CN or DMF), multiple scans or variable scan rates.

[24] a) X. Ottenwaelder, R. Ruiz, R. Ruiz-Garcia, G. Blondin, R. Carasco, J. Cano, D. Lexa, Y. Journaux, A. Aukauloo, *Chem. Commun.* **2004**, 504; b) R. Carrasco, J. Cano, X. Ottenwaelder, A. Aukauloo, Y. Journaux, R. Ruiz-Garcia, *Dalton Trans.* **2005**, 2527.

[25] H.-J. Kruger, G. Peng, R. H. Holm, *Inorg. Chem.* **1991**, *30*, 734.

[26] J. Hanss, H.-J. Kruger, *Angew. Chem. Int. Ed.* **1998**, *37*, 360.

[27] a) R. Ruiz, C. S. Barland, A. Aukauloo, E. Anxolabehere-Mallart, Y. Journaux, J. Cano, M. C. Munoz, *J. Chem. Soc., Dalton Trans.* **1997**, 745; b) B. Cervera, J. L. Sanz, M. J. Ibanez, G. Vila, F. LLoret, M. Julve, R. Ruiz, X. Ottenwaelder, A. Aukauloo, S. Poussereau, Y. Journaux, M. C. Munoz, *J. Chem. Soc., Dalton Trans.* **1998**, 781.

[28] The free ligands do not show any reductive response, which thus suggests that the locus of the reduction is the nickel centre.

[29] T. Storr, E. C. Wasinger, R. C. Pratt, T. D. P. Stack, *Angew. Chem. Int. Ed.* **2007**, *46*, 5198.

[30] The actual oxidizing species suggested with the chemical oxidation by using $Cu(OTf)_2$ is $[Cu(CH_3CN)_4]^{2+}$. See a) M. Inoue, A. R. Mendivil-Sol, H. Grijalya, M. B. Inoue, *Inorg. Chim. Acta* **1989**, *161*, 179; b) C. L. Jenkins, J. K. Kochi, *J. Am. Chem. Soc.* **1972**, *94*, 843; c) S. P. Schmidt, F. Basolo, W. C. Trogler, *Inorg. Chim. Acta* **1987**, *131*, 181.

[31] N. G. Connelly, W. E. Geiger, *Chem. Rev.* **1996**, *96*, 877.

[32] T. R. Wagler, C. J. Burrows, *Tetrahedron Lett.* **1988**, *29*, 5091.

[33] T. Punniyamurthy, S. Velusamy, J. Iqbal, *Chem. Rev.* **2005**, *105*, 2329 and references cited therein.

[34] a) J. Estrada, I. Fernandez, J. R. Pedro, X. Ottenwaelder, R. Ruiz, Y. Journaux, *Tetrahedron Lett.* **1997**, *38*, 2377; b) J. F. Kinneary, J. S. Albert, C. J. Burrows, *J. Am. Chem. Soc.* **1988**, *110*, 6124; c) D. K. Chand, P. K. Bharadwaj, *Inorg. Chem.* **1997**, *36*, 5658; d) S. Murahashi, Y. Oda, T. Naota, *J. Am. Chem. Soc.* **1992**, *114*, 7913; e) J. Haber, T. Mlodnicka, J. Poltowicz, *J. Mol. Catal.* **1989**, *54*, 451.

[35] a) W. Nam, H. J. Kim, S. H. Kim, R. Y. N. Ho, J. S. Valentine, *Inorg. Chem.* **1996**, *35*, 1045 and references cited therein; b) B. B. Wentzel, P. A. Gosling, M. C. Feiters, R. J. M. Nolte, *J. Chem. Soc., Dalton Trans.* **1998**, 2241.

[36] J. F. Kinneary, T. R. Wagler, C. J. Burrows, *Tetrahedron Lett.* **1988**, *29*, 877.

[37] D. T. Sawyer, J. L. Roberts Jr, in *Experimental Electrochemistry for Chemists*, Wiley, New York, **1974**.

[38] *SMART*: *Bruker Molecular Analysis Research Tool*, Version 5.618, Bruker Analytical X-ray System, **2000**.
[39] *SAINT-NT*, Version 6.04, Bruker Analytical X-ray System, **2001**.
[40] *SHELXTL-NT*, Version 6.10, Bruker Analytical X-ray System, **2000**.

Received: October 16, 2007
Published Online: March 13, 2008

